Available online at www.sciencedirect.com
SCIENCE DIRECT®
Physica C xxx (2005) xxx–xxx
PHYSICA C
www.elsevier.com/locate/physc

On heavy carbon doping of MgB_2

Deepa Kasinathan, K.-W. Lee, W.E. Pickett *

Department of Physics, University of California, Davis CA 95616, USA

Received 9 November 2004; accepted 3 May 2005

Abstract

Heavy carbon doping of MgB_2 is studied by first principles electronic structure studies of two types, an ordered supercell ($Mg(B_{1-x}C_x)_2$, $x = 0.0833$) and also the coherent potential approximation method that incorporates effects of B–C disorder. For the ordered model, the twofold degenerate σ-bands that are the basis of the high temperature superconductivity are split by 60 meV (i.e. 7 meV/% C) and the σ Fermi cylinders contain 0.070 holes/cell, compared to 0.11 for MgB_2. A virtual crystal treatment tends to overestimate the rate at which σ holes are filled by substitutional carbon. The coherent potential approximation (CPA) calculations give the same rate of band filling as the supercell method. The occupied local density of states of C is almost identical to that of B in the upper 2 eV of the valence bands, but in the range −8 eV to −2 eV, C has a considerably larger density of states. The calculations indicate that the σ Fermi surface cylinders pinch off at the zone center only above the maximum C concentration $x \approx 0.10$. These results indicate that $Mg(B_{1-x}C_x)_2$ as well as $Mg_{1-x}Al_xB_2$ is a good system in which to study the evolution of the unusual electron–phonon coupling character and strength as the crucial σ hole states are filled.

1. Introduction

Discovery of superconductivity at $T_c \approx 40$ K in MgB_2 has enlivened not only interest in new classes of superconductors with high T_c and novel two-gap behavior, but also pursuit of new materials for applications that require high critical current densities and high critical fields (H_{c2}). In highly resistive films (due to unreacted components and/or oxygen and carbon impurities) the perpendicular and parallel critical fields have reached [1] $H_{c2}^{\perp} \approx 34$ T, $H_{c2}^{\parallel} \approx 49$ T, making MgB_2 a real possibility for a high field conductor. Such application require defects or grain boundaries to pin the vortices whose motion would otherwise lead to energy dissipation and joule heating. Such defects also affect the underlying electronic structure and pairing interaction, at least in some parts of the sample, and often decrease T_c. The simplest defect to understand is the substitutional impurity, which provides a means of varying the intrinsic properties in a

* Corresponding author. Tel.: +1 530 7534123; fax: +1 530 7524717.
E-mail address: pickett@physics.ucdavis.edu (W.E. Pickett).

0921-4534/$ - see front matter © 2005 Elsevier B.V. All rights reserved.
doi:10.1016/j.physc.2005.05.002

continuous and controllable manner and may enhance pinning mechanisms. Although readily synthesizable as a stoichiometric, rather clean compound, the MgB_2 lattice resists most attempts to alloy, both on the Mg and B sites, at more than the very dilute level.

The two established exceptions are Al substitution for Mg, and C substitution for B, both of which lead to a rapid decrease in T_c. Published reports on the behavior vary considerably with synthesis method and sample treatment, but some of the general behavior seems to be established. Al substitution should be the simpler one, since the very strongly bonded honeycomb structure B layers remain intact, and simple rigid band filling of the hole states at first appears to be a likely possibility. Up to $y = 0.10$ in $Mg_{1-y}Al_yB_2$ that appears to be the case, with T_c decreasing smoothly. Beyond the concentration $y = 0.10$, however, there are signs of two-phase behavior (two c lattice parameters in diffraction studies) [2]. Around $y = 0.25$ the system reverts to a single phase very low and finally vanishing T_c. A study of the trends in electron–phonon coupling strength using first principles calculations in the virtual crystal approximation [3] reported a sharp change of behavior at $y = 0.25$. A thorough study of the energetics of Al substitution revealed a strong tendency for superstructure formation [4] at $y = 0.25$ (and $y = 0.75$). Still, the observed onset of two-phase behavior already at $y = 0.10$ is unexplained, and nonstoichiometry [5] and microscopic defects must be kept in mind.

Unlike the Al alloying case where there has been at least rough consensus on changes of properties, reports of the change in T_c and structure with addition of carbon on MgB_2 have varied widely. These differences seem in some cases to reflect real differences in materials due to the various methods of synthesis and heat treatment, and the samples prepared were highly mixed phase, thereby creating additional uncertainty. The very similar X-ray scattering strength of the B and C atoms has rendered standard X-ray diffraction ineffective in determining the C content of a sample. Reports early on suggested C miscibilities in $Mg(B_{1-x}C_x)_2$ as small [6] as $x = 0.02$ to as large [7] as $x = 0.3$. Recent studies of several groups suggest that $x = 0.2$ can be achieved while larger concentrations are questionable [8–10] although reports of larger C concentrations under high pressure growth persist [11].

With some of the materials questions coming under control, the observed trends are raising some serious questions. The decrease in T_c follows $dT_c/dx \sim 1$ K/% C [12], with several reports of $T_c \approx 21$–23 K at $x = 0.2$ [8–10]. However, with carbon adding one electron and the σ-bands of MgB_2 holding only ~0.11 holes per unit cell [13], one might guess that the σ-bands would be filled (or nearly so, as the π-bands can also accept carriers) and superconductivity would have vanished. Not only is T_c still robust at $x = 0.2$, analysis of tunneling spectra indicates two-band superconductivity is retained [14,15], whereas it might also seem likely that disorder scattering should have averaged out the gap to a single value. The upper critical field H_{c2} initially increases strongly with C content as T_c is depressed, reaching a maximum [1,12,16] of ~33–35 T. This critical field is substantially less than that for more disordered films (see above).

Recent studies seem to agree that C can be introduced substitutionally for B up to 10% replacement $x = 0.10$ [8,17]. Tunneling spectroscopies indicate that $Mg(B_{1-x}C_x)_2$ remains a two-gap superconductor [8,14] (i.e. the gap anisotropy is not washed out by scattering) for $10 \pm 2\%$ C substitution for B. This question of how the anisotropy gets washed out has attracted much interest. Similarly, the mechanisms underlying the high critical fields are not understood. These questions are not the focus of the present study, although the knowledge gained from first principles calculations will be useful in the resolution of these topics.

A few first principles calculations have been done for C substitution of B in MgB_2. Pseudopotential calculations including relaxation in a 27 unit cell supercell [18] confirmed that substitutional C is energetically favorable to interstitial C, and that the C–B bond length is 5–6% shorter than the bulk B–B bond length. A projector-augmented-wave calculation [19] reported a smaller relaxation, but the difference may be due to constraints related to supercell size. A coherent poten-

tial approximation study of the disordered alloy using a Korringa–Kohn–Rostoker multiple scattering method in the atomic sphere approximation [20] revealed relatively small effects of disorder in the range $0 \leqslant x \leqslant 0.3$. The main effect of C substitution was reported to be the raising of the Fermi energy due to the additional carriers, but the filling of the crucial σ hole band was not quantified.

In this paper, we present a more detailed analysis of the changes in electronic structure, and the effective σ-band doping, using both periodic supercells and disordered alloy calculations. Our study lays the groundwork for another issue in the superconductivity of MgB_2 alloys that has received no direct attention from experimentalists: the effect of decreasing holes on the strength and character of electron–phonon coupling. Theoretical studies [21–23] have predicted the following remarkable changes in doped MgB_2: as the number of holes decreases (hence the Fermi wavevector k_F of the cylindrical σ Fermi surfaces decreases), (1) the substantial downward renormalization of the E_{2g} bond-stretching modes with $Q \leqslant 2k_F$ does not change, (2) the coupling strengths of these already strongly coupled modes increases, and (3) the total coupling strength λ, and hence T_c, remains unchanged. This scenario assumes two-dimensionality of the σ-bands which is only approximately true, and neglects the change of electron–phonon matrix elements which should be reasonable. This argument also neglects the fact that the applicability of conventional electron–phonon (Midgal–Eliashberg) theory, already somewhat suspect [24,25] in MgB_2, definitely becomes inapplicable as the Fermi energy decreases and approaches more closely the bond-stretching mode energy (65 meV). Item (2) definitely portends unusual dynamics related to the B–B stretch modes. We hope the current paper stimulates experimental investigation into these questions.

2. Calculational methods

Two methods of assessing the effects of substitutional C in MgB_2 have been used in the work reported here. Our ordered impurity calculations have been performed using the full-potential linearized augmented plane wave code Wien2k [26], applying the generalized gradient approximation [27] to the exchange-correlation potential. The basis set is reduced by using the APW + lo method [28], retaining the accuracy of the LAPW method. RK_{max} was set to 7.00 which is a high quality basis for the s–p electron systems. The Brillouin zone integration for the supercell was carried out using 432 k points in the irreducible part of the zone. We have used the experimental results of Avdeev et al. [17] for the lattice parameters of the 8.33% doped supercell and the 10% doped virtual crystal (Table 1).

Table 1
Lattice parameter values used in the virtual crystal and supercell calculations

Lattice parameter	Undoped MgB_2 (Å)	10% Doping $MgB_{1.8}C_{0.2}$ [17] (Å)	8.33% Doping $Mg_6B_{11}C$ (Å)
a	3.083	3.053	$3 \times 3.053 = 49.159$
b	3.083	3.053	$2 \times 3.053 = 6.106$
c	3.521	3.525	3.525

For the disordered (randomly substituted) alloy calculations, we have used the full-potential non-orthogonal local-orbital minimum-basis scheme (FPLO) [29] applied in the coherent potential approximation (CPA) [30]. In the calculations, 1152 ($45 \times 45 \times 10$) irreducible k points, and valence orbitals 2s2p3s3p3d for Mg and 2s2p3d for B and C, were used. The implementation of the CPA in FPLO relies on the Blackman–Esterling–Berk theory [31] that includes random off-diagonal matrix elements in the local-orbital representation.

3. Ordered $Mg(B_{1-x}C_x)_2$, $x = 0.0833$

Smaller concentrations of ordered C substitution for B require larger supercells. Our choice of supercell was guided by the desire for a small enough C concentration to be relevant to address experimental data, yet not so small as to make it difficult to distinguish the effect of C addition or to make the calculations unreasonably tedious. Since interlayer hopping is not an issue we will address, the supercell will involve enlargement of only a single B layer. The shape of supercell should

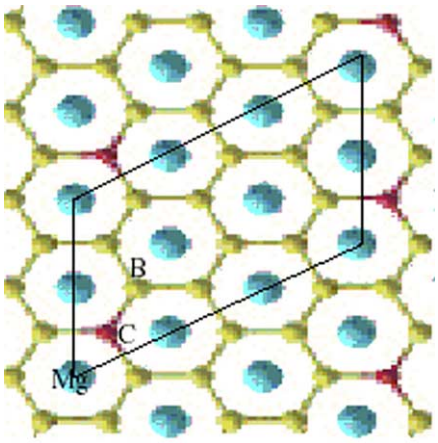

Fig. 1. Top view of the B–C layer of the $Mg_6B_{11}C$ supercell. Large (blue) circles denote Mg atoms, small light (yellow) circles denote boron, and small dark (red) circles denote carbon. The supercell boundary is outlined. (For interpretation of the references in colour in this figure legend, the reader is referred to the web version of this article.)

have as small as possible aspect ratio in order to maximize the separation of C atoms. The compromise we chose was the 8.33% doped supercell ($Mg_6B_{11}C \rightarrow Mg(B_{1-x}C_x)_2$, $x = 1/12 = 0.0833$). Fig. 1 shows the top view of the $B_{11}C$ layer in the 2×3 supercell. Each carbon atom has three first, five second, and three third nearest neighbor boron atoms.

3.1. Band structure

There are two effects of carbon substitution: a change in the average potential in the B–C layer, and the breaking of symmetry by C replacement of B in the supercell. In the ordered supercell the potential difference is kept explicit and symmetry breaking will be clear. In Section 6 CPA will be used to probe these effects in a different manner. Another effect, B relaxation around the C impurities, has been addressed previously to some extent, but it will not be studied here since the effect cannot be included within the CPA.

The band structure within 4 eV of the Fermi level (E_F) is shown in Fig. 2. The primary band in the understanding of MgB_2 superconductivity is the (twofold degenerate) σ-band along the Γ–A direction. The results of supercell band-folding

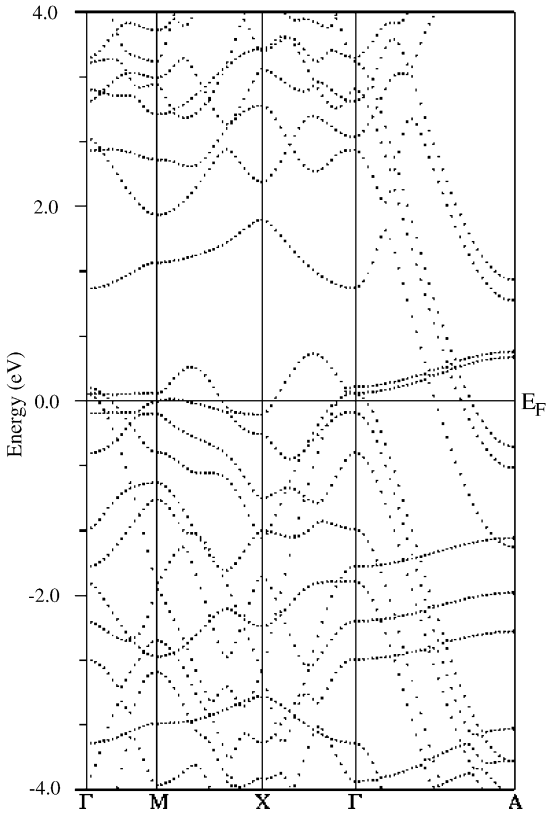

Fig. 2. Band structure of $Mg_6B_{11}C$ in the region of the Fermi level. The twofold degenerate σ-band in the undoped system along the Γ–A is split by 60 meV when 1/12 of B is replaced by C.

can be distinguished especially for the Γ–A direction, where (for example) the σ-band dispersion is replicated at Γ at -1.8 eV, -2.3 eV, -2.6 eV, and even further lower energies.

One of the most readily apparent effects of C doping is the splitting of the σ-bands along Γ–A, by 60 meV. It is helpful in understanding this splitting to obtain the atomic characters of each of the split bands, which will in any case involve only the B and C p_σ (p_x, p_y) states. The carbon p contribution is emphasized by enlarged symbols (''fat-bands'') in Fig. 3. The lower of the two bands has stronger C content (although this is not easy to distinguish in Fig. 3). In addition, it has more first and second B neighbor character than does the upper band. The upper band contains more third neighbor B character, this being the B site

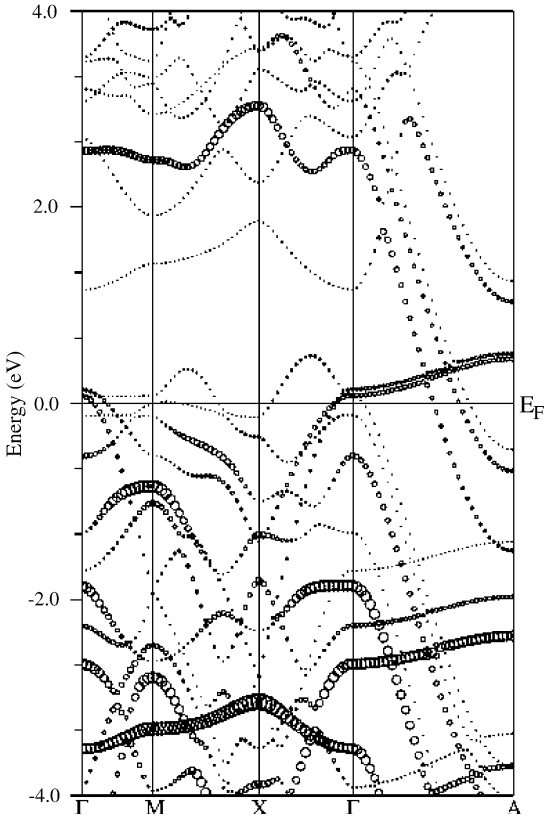

Fig. 3. Bands of $Mg_6B_{11}C$ near the Fermi level, with symbol size proportional to the C 2p character. The σ-bands, split by 60 meV (hardly visible in this figure) lie just above E_F at Γ and disperse upward toward the A point.

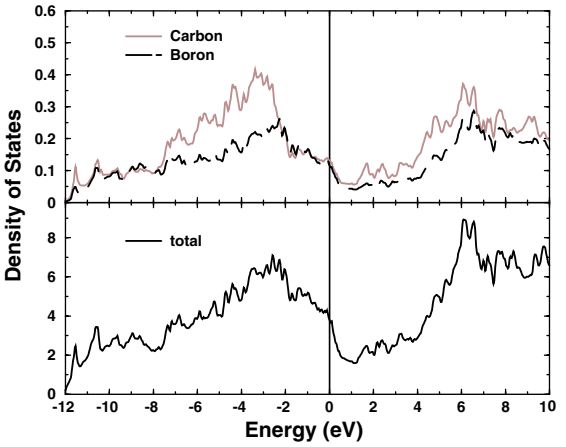

Fig. 4. Density of states, total (bottom) and decomposed into B and C contributions on a per-atom basis, for the ordered $x = 1/12$ model. The primary B–C difference is that the C DOS is lower in the −2 eV to E_F region, but higher in the lower region −8 eV to −2 eV.

farthest from the C atom and representative of the bulk material. The interpretation of this splitting is that lower band has been pulled down due to the stronger potential of the C atom compared to that of B. The 60 meV splitting for $x = 1/12$ provides (assuming a linear effect in this concentration range) an energy scale for σ-band broadening $\gamma_0 \approx 7$ meV/% C content.

3.2. Density of states

Fig. 4 shows the total and atom-projected density of states (DOS) of the 8.33% doped system. The C and B DOS are similar at and above E_F, but the C DOS is somewhat lower in the interval within 2 eV below E_F. The C DOS is larger than that of B in the −8 eV to −3 eV region. Based on charge within spheres of 1.65 Å radius we calculated a charge transfer of about $0.095e^-$ to the carbon from the three first nearest neighbor boron atoms, with other B sites showing negligible change in charge. This charge transfer also reflects the stronger potential and larger electronegativity of C, and provides substitutional C with definite anionic character.

4. 10% Doping

We have also performed a virtual crystal approximation (VCA) calculation for the 10% doped $x = 0.10$ system $Mg(B_{0.9}C_{0.1})_2$. The DOS and band structure are shown in Figs. 5 and 6. By aligning the highest peaks in the DOS at −2 eV and +6 eV (they can be aligned simultaneously), we establish that the differences are (1) an increase in the occupied bandwidth (at the MgB_2 band filling) from 12.4 eV to 12.5 eV (∼1%), and (2) the raising of the Fermi level by 0.3 eV to accommodate the extra electrons. Otherwise there is very little difference in the two densities of states. This raising of E_F will be compared to the supercell result in the next section. At this band filling, the VCA gives the σ-band edge at Γ

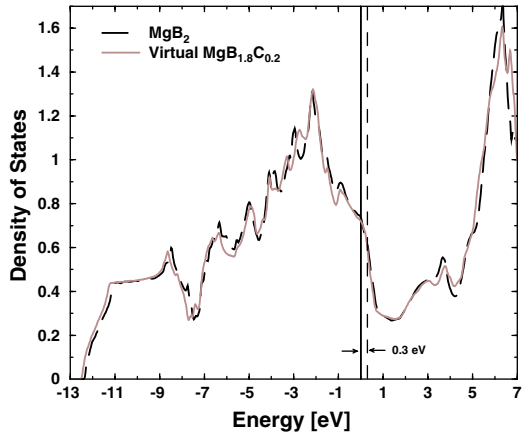

Fig. 5. Density of states of $Mg(B_{0.9}C_{0.1})_2$. The Fermi level moves up by 0.3 eV due to doping.

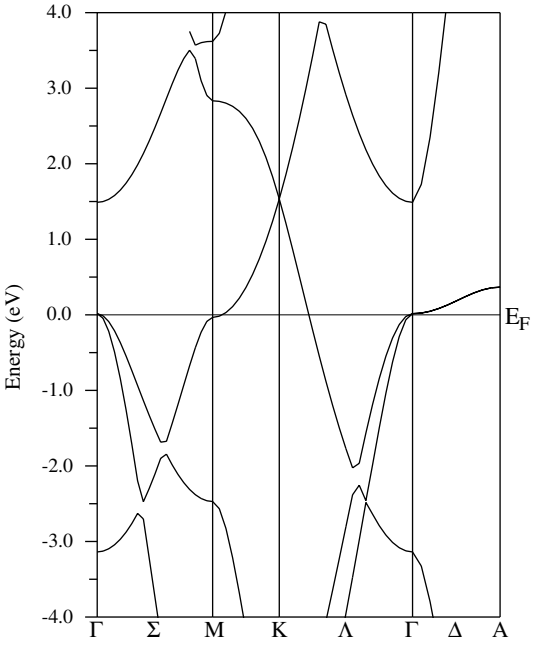

Fig. 6. Band structure of $Mg(B_{1-x}C_x)_2$, $x = 0.10$, in the virtual crystal approximation. The σ-bands at Γ lie precisely at E_F, so the Fermi cylinder radii at Γ vanish, corresponding to a topological transition.

precisely at E_F as shown in Fig. 6. At the point A it is still about 0.3 eV above E_F, meaning that both cylindrical Fermi surfaces have shrunk to a point at their "waists."

5. σ hole concentration

It is accepted that superconductivity in MgB_2 arises from hole-doping of the σ bonding hole states due to the intrinsic chemistry [13] of MgB_2. The observed decrease in electron–phonon coupling strength, and hence T_c upon C addition, makes the change in hole concentration one of the major points of interest. We have calculated the hole concentration of both the 8.33% supercell system and the 10% virtual system from the volume enclosed by the Fermi surface. Since the radii of the cylindrical Fermi surfaces are only slightly different along the $\Gamma \rightarrow M$ and the $\Gamma \rightarrow K$ directions, we calculated the average basal area by considering the value along the $\Gamma \rightarrow M$ direction only. Also, we assumed a sinusoidal dependence of the Fermi surface along the $\hat{c}$ axis, allowing analytic evaluation of the Fermi surface volumes i.e. the hole concentrations. The results are presented in Table 2. In the process of calculating the number of holes, electronic structure reveals that both the σ-band Fermi surfaces are still intact, consistent with the two-band superconductivity with substantial T_c as seen in experiments [8]. Also, we interpolated the number of holes for the 10% doped system (virtual crystal) to calculate the value for the 8.33% doped system. Supercell calculation gave 0.070 holes/cell while the extrapolation gave only 0.057 holes/cell. This indicates that the virtual crystal approximation is not very reliable for substitutional carbon, and that C cannot be thought of "boron + an electron."

6. Coherent potential approximation results

For further comparison and to assess the effects of disorder, we have performed CPA studies of

Table 2
Calculated number of σ holes for the various C concentrations discussed in the text

	No. of holes (holes/cell)
MgB_2	0.11
8.33% Doping $Mg_6B_{11}C$ supercell	0.070
10% Doping $MgB_{1.8}C_{0.2}$ virtual crystal	0.0463
8.33% Doping $MgB_{1.833}C_{0.167}$ extrapolation	0.057

this system. We have carried out CPA calculations (1) at $x = 0.0001$ to provide a "perfect crystal" reference for evaluation of the various algorithms in the CPA code, (2) at $x = 0.0833$ for most direct comparison to the $x = 1/12$ (ordered) supercell calculations described in the previous sections, and (3) at $x = 0.10$ and 0.20 as representative of the system toward the upper range of achievable C substitution. The spectral function over the whole energy range of interest, plotted as a "smeared" band structure, is shown for the $x = 0.20$ case in Fig. 7. The primary points of interest are the filling of the σ-band hole states, and the broadening (and potentially splitting) of bands.

The full energy region is presented in Fig. 7 for $x = 0.20$ (where broadening is more easily seen) to illustrate the strong wavevector (k) and energy (E) dependence of the broadening of the spectral function. The largest disorder occurs in the 2s region in the lower valence band, where the C 2s state is noticeably lower in energy leading to increased smearing. The other region of large disorder is from +3 eV upward, but some states remain comparatively sharp. The flat band at 5 eV along Γ–M and A–L, with strong π character, is the lowest conduction band that is strongly affected by the disorder. The bands around the Fermi level, whether σ or π, are among those less affected by the chemical disorder. As expected from the virtual crystal results for $x = 0.10$ from the previous section, the σ-band holes are completely filled at $x = 0.20$, as revealed by the flat band along the Γ–A line lying entirely below E_F. The band filling behavior versus x is quantified below.

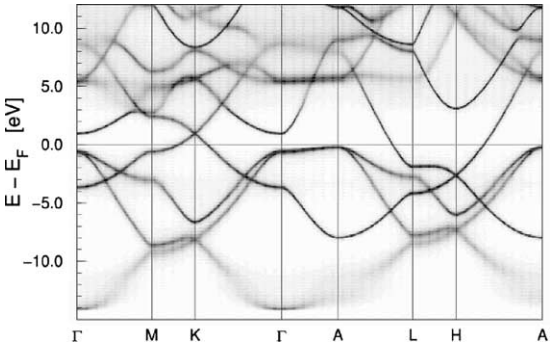

Fig. 7. CPA spectral density in the full valence–conduction band region, for $x = 0.20$, plotted as a broadened band structure. Disorder broadening is largest below −8 eV in the valence bands and above 4 eV in the conduction bands.

In the valence (occupied) bands, disorder broadening is large in the lower s-band region −8 eV to −14 eV below E_F, and somewhat less so where the (primarily σ) band in the −3 to −4 eV range gets flat around the zone edge M and L points. Similar broadening does not occur in the same band at the (more distant from Γ) zone edge K and H points, where the band lies at −6 eV and is much less flat. The top of the σ bonding bands along Γ–A are comparatively sharp; the width is quantified below.

In the conduction bands disorder broadening becomes more prevalent. The antibonding σ*-bands (flat along Γ–A at +6 eV) are much broader than their bonding counterparts (below E_F), and this band along Γ–M and A–L with Mg 3s character becomes exceedingly diffuse. The π-bands show strong k-dependence of the broadening, beginning at 2–3 eV around the M point and becoming wider in the 6–10 eV range (and above, not shown in the figure).

6.1. Carbon concentration dependence

The x-dependence of the broadening can be seen in Fig. 8 for $x = 0.0001$ (the CPA equivalent of $x = 0$ MgB_2), for $x = 0.10$, and for $x = 0.20$ (the latter may not be experimentally accessible). Since in each case E_F is set to zero, band filling appears as downward shifts of the bands, by roughly $\delta E_F = -0.4$ eV for $x = 0.10$ and $\delta E_F = -1.0$ eV for $x = 0.20$. For $x = 0.0833$ (not shown) the σ-bands lie at the same position (with respect to E_F) as for the ordered $x = 1/12$ case shown in Fig. 3. Hence the degree of band filling in the CPA results is the same as for the ordered $x = 1/12$ case that was analyzed in the previous section. Although we will not dwell on it, it can be noticed that the band shift is not entirely rigid: the two valence bands at the L point split apart as well as broaden with increasing C concentration.

The other important aspect of the CPA bands of Fig. 8 is the broadening that increases with carbon concentration. Within the resolution of widths that we are able to extract, the widths of the

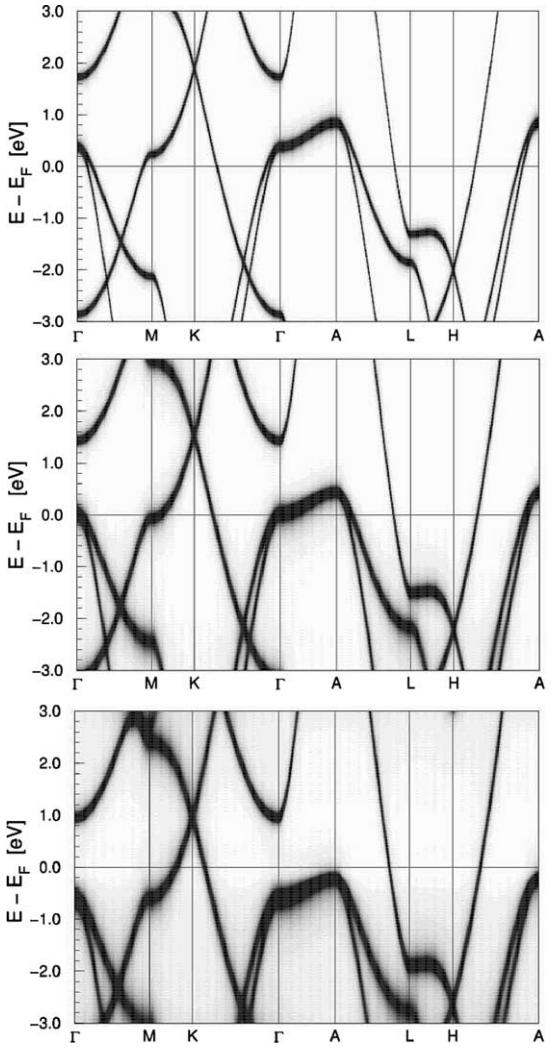

Fig. 8. CPA spectral density for $x = 0.0001$ (top panel), $x = 0.10$ (middle) and $x = 0.20$ (bottom panel). The main features are (i) the "rising" Fermi level (with respect to the σ-band along Γ–A, say), and (ii) the increase in the disorder broadening of the bands. Since the numerical algorithms cannot reproduce the δ-function bands for $x \to 0$, the $x = 0.0001$ case is included as a reference for the algorithmic contribution to the width.

σ-bands can be taken to be proportional to x, but differ considerably between Γ and A (being about 50% wider at Γ). The full width at half maximum of the spectral density of the σ-bands, averaged between Γ and A, is about $\gamma \approx 0.21$ eV (to perhaps 10% accuracy). This width corresponds to a width in wavevector given by $\gamma = v_F \delta k$, and therefore a mean free path of $\ell_F = 2\pi v_F/\gamma$. The 60 meV splitting of the σ-bands (see Section 3.1) for the $x = 1/12$ ordered supercell implies that the 0.21 eV mean width can be interpreted as 0.06 eV from the B/C on-site energy difference, and thus 0.15 eV from disorder itself.

Due to the anisotropy of the Fermi velocity v_F, the mean free path may vary considerably over the Fermi surface at $x = 0.10$. At Γ the cylinder radius has shrunk to a point, and the very small z component of v_F (vanishing at Γ) suggests a very small mean free path in the z direction of the order of the layer spacing c for $x = 0.10$.

7. Discussion and summary

In the band structure of the 8.33% doped supercell system, the hole σ-band Fermi surfaces along the $\Gamma \to A$ direction are still present, and this degree of band filling is reproduced by the CPA. Even for $x = 0.10$ the virtual crystal picture (which overestimates the rate of band filling by C) leaves σ Fermi surfaces, just beginning to be pinched off. The CPA calculations (Fig. 8) show the σ-band holes begin to disappear rapidly for $x > 0.10$. Qualitatively this filling is consistent with most experimental reports.

The questions, and experimental probes, should now be focused on the fact that, as the σ-band fills, there will be very strong deviation from 'business as usual' in the coupled electron–phonon system. The strength of coupling of bond-stretching modes with $Q < 2k_F$ continues to increase, and conventional Migdal–Eliashberg theory ceases to apply. The dynamics of these ultra-strongly coupled modes is unexplored, with their peculiar character being signaled by the divergence of their linewidth (at least within Migdal–Eliashberg theory). The limiting behavior should not revert to the widely studied polaron limit, however, as there remain the background π electrons, which are weakly coupled to vibrations but provide full metallic conductivity and screening to the system. The present study reveals that C substitution for B provides a similarly favorable system to Al substitution for Mg for studying this evolution. Recent reports

indicate that Sc substitution ($Mg_{1-x}Sc_xB_2$) may also provide [32] another such system for study.

Acknowledgements

We acknowledge communication on the topics of this paper with P. C. Canfield, L. C. Cooley, K. Koepernik, I. I. Mazin, and D. J. Singh. This work was supported by National Science Foundation Grant DMR-0421810.

References

[1] A. Gurevich, S. Patnaik, V. Braccini, K.H. Kim, C. Mielke, X. Song, L.D. Cooley, S.D. Bu, D.M. Kim, J.H. Choi, et al., Supercond. Sci. Technol. 17 (2004) 278.
[2] J.S. Slusky, N. Rogado, K.S. Regan, M.A. Hayward, P. Khalifah, T. He, K. Inumaru, S.M. Loureiro, M.K. Haas, H.W. Zandbergen, et al., Nature 410 (2001) 343.
[3] G. Profeta, A. Continenza, S. Massidda, Phys. Rev. B 68 (2003) 144508.
[4] V. Barabash, D. Stroud, Phys. Rev. B 66 (2002) 012509.
[5] U. Burkhardt, V. Gurin, F. Haarmann, W.S.H. Borrmann, A. Yareskko, Y. Grin, J. Solid State Chem. 177 (2004) 389.
[6] I. Maurin, S. Margadonna, K. Prassides, T. Takenobu, Y. Iwasa, A.N. Fitch, Chem. Mater. 14 (2002) 3894.
[7] A. Bharathi, S.J. Balaselvi, S. Kalavathi, G.L.N. Reddy, V.S. Sastry, Y. Hariharan, T.S. Radhakrishnan, Physica C 370 (2002) 211.
[8] H. Schmidt, K.E. Gray, D.G. Hinks, J.F. Zsadzinski, M. Avdeev, J.D. Jorgensen, J.C. Burley, Phys. Rev. B 060508 (2003) 68.
[9] M. Andeev, J.D. Jorgensen, R.A. Ribiero, S.L. Bud'ko, P.C. Canfield, Physica C 301 (2003) 387.
[10] R.A. Ribiero, S.L. Bud'ko, C. Petrovic, P.C. Canfield, Physica C 16 (2003) 385.
[11] T. Masui, S. Lee, S. Tajima, Phys. Rev. B 70 (2004) 024504.
[12] R.H.T. Wilke, S.L. Bud'ko, P.C. Canfield, D.K. Finnemore, R.J. Suplinskas, S.T. Hannahs, Phys. Rev. Lett 92 (2004) 217003.
[13] J.M. An, W.E. Pickett, Phys. Rev. Lett. 86 (2001) 4366.
[14] Z. Holanova, P. Szabo, P. Samuely, R.H.T. Wilke, S.L. Bud'ko, P.C. Canfield, Phys. Rev. B 70 (2004) 064520.
[15] P. Samuely, Z. Holanova, P. Szabo, J. Kacmarcik, R.A. Ribiero, S.L. Bud'ko, P.C. Canfield, Phys. Rev. B 68 (2003) 020505.
[16] R. Puzniak, M. Angst, A. Szewczyk, J. Jun, S.M. Kazakov, J. Karpinski, cond-mat/0404579 (2004).
[17] M. Avdeev, J.D. Jorgensen, R.A. Robeiro, S.L. Bud'ko, P.C. Canfield, Physica C 387 (2003) 301.
[18] Y. Yan, M.M. Al-Jassim, J. Appl. Phys. 92 (2002) 7687.
[19] S.C. Erwin, I.I. Mazin, Phys. Rev. B 68 (2002) 132505.
[20] P.P. Singh, Solid State Commun. 127 (2003) 271.
[21] J.M. An, H. Rosner, S.Y. Savrasov, W.E. Pickett, Physica B 328 (2003) 1.
[22] W.E. Pickett, J.M. An, H. Rosner, S.Y. Savrasov, Physica C 387 (2003) 117.
[23] Y. Kong, O.V. Dolgov, O. Jepsen, O.K. Andersen, Phys. Rev. B 64 (2001) 020501.
[24] L. Boeri, G.B. Bachelet, E. Cappelluti, L. Pietronero, Phys. Rev. B 65 (2002) 214501.
[25] W.E. Pickett, Braz. J. Phys. 33 (2003) 695.
[26] P. Blaha, K. Schwarz, G.K.H. Madsen, D. Kvasnicka, J. Luitz, J. Phys. Chem. Sol. 63 (2002) 2201.
[27] J.P. Perdew, K. Burke, M. Ernzerhof, Phys. Rev. Lett. 77 (1996) 3865.
[28] E. Sjostedt, L. Nordstrom, D.J. Singh, Solid State Commun. 114 (2000) 15.
[29] K. Koepernik, H. Eschrig, Phys. Rev. B 59 (1999) 1743.
[30] K. Koepernik, B. Velicky, R. Hayn, H. Eschrig, Phys. Rev. B 55 (1997) 5717.
[31] J.A. Blackman, D.M. Esterling, N.F. Berk, Phys. Rev. B 4 (1971) 2412.
[32] S. Agrestini, C. Metallo, M. Filippi, L. Simonelli, G. Campi, C. Sanipoli, E. Liarokapis, S.D. Negri, M. Giovannini, A. Saccone, et al., Phys. Rev. B 70 (2004) 134514.